



## Effective Power Flow Control of Grid Tied Hybrid Renewable Energy System Using SMC Controller

Abousserhane Zakaria<sup>1\*</sup>      Abbou Ahmed<sup>1</sup>      Bouzakri Hicham<sup>1</sup>

<sup>1</sup>*Mohammadia School of Engineers, Mohammed V University in Rabat, Morocco*

\* Corresponding author's Email: zakariaabousserhane@research.emi.ac.ma

---

**Abstract:** The aim of this paper is developing and validating the sliding mode control application (SMC) for hybrid renewable energy system (HRES) featuring stand-alone and on-grid operations modes. The proposed system composed by a photovoltaic (PV) and wind turbine (WT) as principal sources. The PV is connected to the overall system via boost converter which controlled using MPPT algorithm depending to Adaptive Perturb and Observe (APO) method managed by SMC to extract maximum of power of PV modules. The WT depends to a Permanent Magnet Synchronous Generator (PMSG) and a controlled rectifier to maximize the operating point of the WT. Therefore, the battery and supercapacitors are connected to the system via a bidirectional converter to ensure the charging modes operations. The voltage source converter (VSC) is controlled by SMC had an aim to control the frequency and amplitude of the system outputs injected into the grid and load utility. To expose the performance of the proposed sliding mode control approach, we propose a different comparatives tests include a conventional PI control and hysteresis current control under two operating grid modes depending to different climate scenarios. The developed control strategy for HRES have shown great results such as the control performance, effectiveness and delivers low harmonic distortion values (Max of THD are 3,43% and 4,88%) compared with hysteresis current controller (Max of THD are 4,63% and 10,98%) and PI control (Max of THD are 4,92% and 12,86%) featuring OFF and ON grid, respectively. Finally, the proposed control enhances the HRES quality and stability.

**Keywords:** Hybrid system, Photovoltaic, Wind turbine, Battery, Supercapacitor, Energy management, Grid, Sliding mode control.

---

### 1. Introduction

The hybrid interconnected Renewable Energy Resources (RES) and storage systems can increase the energy presence and maximize the power generation systems basing on different points of view [1]. In the last years, the hybrid PV, WT, battery and super-capacitor systems have a great cost-competitive and innovative solution used in both stand-alone and grid-connected applications [2]. Newly, the PV and wind generators are using in many human life domains. To enhance the availability and optimize the power generation of this kind of systems, it is necessary to add a storage system. The researches realized in [3, 4] about the optimization, power management and control of hybrid renewable systems, they confirm that the

effectiveness of a PV & WT hybrid system is more performant than only photovoltaic system [5, 3]. Also, they sensualize to associate the two sources PV/WT with battery energy storage, it can provide many benefits compared to each one only, which can produce more of energy with low greenhouse gases [4]. In other parts, the uses of hybrid systems have become important because the solar and wind resource are free and available in different places and the installation costs are becoming low. In other part, to reinforce and develop these hybrid sources, it can use a super-capacitor, fuel cells or diesel generator under low climatic conditions and fabless battery time [6, 7].

The PV system is composed by power elements like the PV modules tied to the DC bus by DC boost controlled by a maximum power point tracking control. The aim of this control is maximizing the

output PV power of the panels under different solar irradiance conditions. The incremental conductance and perturb & observe are the most MPPT techniques used because they have a simple structure for well understanding and implementation [6-8]. In other hand, the MPPT algorithms are incapable to predict the MPP under quick varying conditions which reduce their performance. Furthermore, the proposed solution of this problem depends to the P&O classic MPPT algorithm tied in cascade with PV generator voltage or current using PI regulator [8-10]. The proposed APO maximum power point tracking control application with an adaptive gain provide an acceptable dynamic performance to follow the MPP under different solar radiations [10]. In this article, we applied the developed APO control to the boost converter to extract the maximum of PV output power, which we used a two-stage control structure using the classic PO algorithm and an developed gain cascade algorithm with a voltage regulator based on a SMC regulator [8].

Lastly, the wind turbine applications are highly using the Permanent magnet synchronous generators which is used for different scenarios like offshore wind power generation complexes which deliver high capacity, cost efficiency and easy maintenance management. The PMSG present many advantages like the low production costs due to developed process used in this technology and low generator weight and low maintenance costs. Also, they can produce a high torque output compared to doubly-fed induction generators caused by the density and the high magnetic flux efficiency. [11-13]

The battery is connected to the DC bus side via DC bidirectional converter, which can ensure the storage operations. The battery control depends to different traditional like PI and hysteresis regulators, their compartment is more discussed in [14, 15], it is very simple and based on generation of high amplitude oscillations which had a nice effect on the quality and performance of the considered system [14, 15], the authors in [15] present the advantages of the linear PI regulator for battery current regulation, it has simple implementation, and in the opposite, it hasn't a high stability under quick variation of weather conditions.

This work tries to design a new control strategy compatible with the HRES which contains PV, WT, battery and SC. For that, we try to explain and find out the contribution of this controller method applicated on the proposed system, the definition of the SMC was explained as a non-linear kind of regulator which introduced to control the variable of designed systems. Besides that, it has many

advantages such as the high stability and robustness [16] which it is considered as a suitable control of power converters for the hybrid system.

Moreover, this work treats a sliding mode control applied on HERS under stand-alone grid mode and grid ON mode. The Fig. 1 shows a schematic of the WT, PV, battery and SC system composition. The PV panels are interfaced to the system side via DC boost converter, this converter is controlled by APO as MPPT control to extract the maximum of PV power under variable climate conditions. The WT is connected to PMSG which is coupled to the DC-bus via VSC, the last one is controlled using SMC. The battery is tied to the system via bidirectional converter adapted by SMC controller and the SC is connected by DC-DC bidirectional converter, the aims of the SC is equilibrated difference between the generated power and consummated power, it is the responsible on the fluctuation absorption into the system which reduce the battery stress. The VSI is the link transformer between DC bus, grid and AC load, it is the responsible of power sharing between system components depending to the operations modes, this converter is managed by SMC regulator.

The main advantages of the proposed control scheme over other the existed are: the analysis of the control scheme SMC for PV/WT/SC/battery featuring two grid modes (ON and OFF modes), was attempted for the first time in this work; the developed SMC for VSC injects power into the grid with good tracking indices and with a low THD (inferior to 5%); the proposed SMC control method has undeniable contributions such as the injected current quality and voltage regulation to the loads under different scenarios balanced and unbalanced load. The developed SMC control strategies for the different power converters have ensured stable operation of the HRES under different operating conditions.

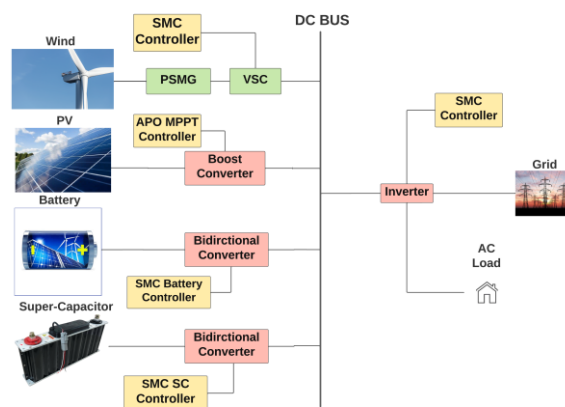


Figure. 1 Proposed hybrid system schematic

The paper organization starts with detailing and modelling of the PV system, wind turbine, battery and supercapacitors. The second part describe and define the proposed system control which composed the APO MPPT algorithm, PSMG control, battery, SC and the VSI control. The latest part contains the simulation results and discussion to show the advantages and importance of the proposed control strategy on the HRES stabilization.

## 2. System under consideration:

### 2.1 PV system modelling:

The photovoltaic cells generators are the main components of PV panels, which it is composed by photocurrent coupled to diode, shunt (RL) and series (Rs) resistances. Furthermore, the proposed equivalent solar cell circuit is illustrated in Fig. 2, the next expressions resume the properties of the photovoltaic generator. The output current of solar cell can be expressed using Kirchoff's law: [17]

$$I = I_{ph} - I_d - \frac{V+I \times R_s}{R_p} \tag{1}$$

Where: the diode current (Id) and voltage (V). The diode current can be calculated by the next equation:

$$I_d = I_0 \left[ \exp \left( \frac{q(V+I \times R_s)}{N_s a k T} \right) - 1 \right] \tag{2}$$

The output current of the PV cells can be modelled following the next equation: [11]

$$I = I_{ph} - I_0 \left( e^{\frac{q(V+R_s \times I)}{nKT}} - 1 \right) - \frac{V+I R_s}{R_p} \tag{3}$$

Where:

I<sub>ph</sub>: Photo-current depends to the incoming sun rays.

I<sub>0</sub>: the reverse saturation current (A), K: Boltzmann constant equal  $1.381 \times 10^{-23}$  (j/k).

q: electron charge equal  $1.6 \times 10^{-19}$  (C).

T: the cell temperature (K).

V: the cell voltage (V).

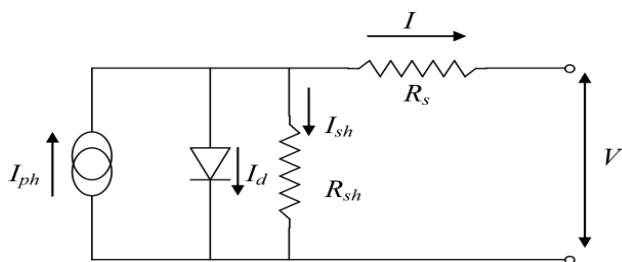


Figure. 2 Electrical solar cell circuit

Table 1. PV module information's

Parameters	Values
Open Circuit Voltage	90,5V
Short Circuit Current	6,21 A
Maximum Voltage (VMPP)	76,7V
Maximum Current (IMPP)	5,8 A
Cells Per Module	128 cells

The used solar PV modules of this work are SunPower SPR-X-20-445e-COM” produced using a polycrystalline silicon material with 445W as maximum of power. Besides that, the table (1) shows the PV electrical parameters of each solar modules.

### 2.2 Wind system modelling:

The wind turbine mechanical power can describe following the Eq. (4), it's depended to air density ( $\rho$ ), the wind speed ( $v_w^3$ ), the wind turbine rotor radius ( $r_t$ ) and the power coefficient ( $C_p(\lambda, \beta)$ ):

$$P_m = \frac{1}{2} \rho \pi r_t^2 C_p(\lambda, \beta) v_w^3 \tag{4}$$

The Fig. 4 shows that the power coefficient depends to two important parameters  $\lambda$  and the pitch angle  $\beta$ , it is mentioned that the Cp reach only optimal point at ( $\lambda_{max} = 0,48, \beta = 0$ ). [18]

Therefore, the Fig. 4 illustrates the wind turbine output of the mechanical power under varying rotational speeds. For more performance precision, the red curve presents the maximal power produced by the wind turbine. Besides that, the Table 2 resume the technical information's of the used WT in this paper.

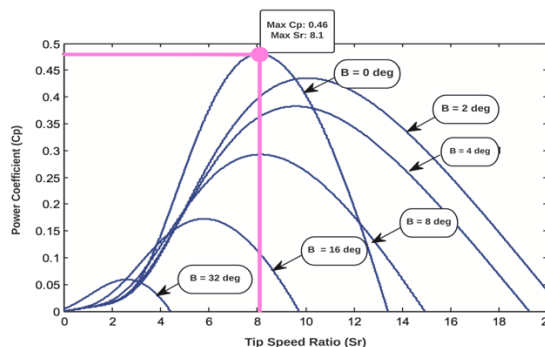


Figure. 3 Power coefficient under different pitch angle

Table 2. Technical information's of WT

Parameters	Values
Power Maximal	10 KW
Speed Maximal	12 m/s
Area Swept by Blades	02 m
Optimum Tip Speed Ratio	08.1

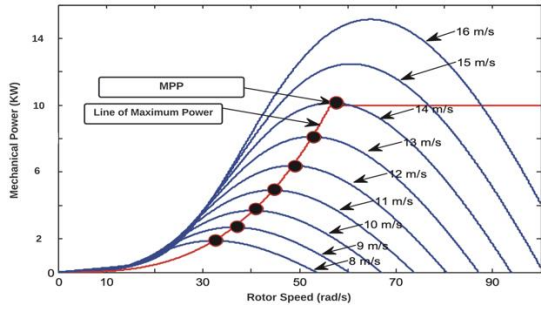


Figure. 4 Performance of wind turbine under varying wind speeds

Due to the variable wind speed and their low rotational synchronous speeds, it is necessary to connect the WT by PMSG. Therefore, the PMSG currents in d-q reference can be described using the next electrical equation:

$$\begin{cases} \frac{dI_{sd}}{dt} = -\frac{R_s}{L_s}I_{sd} + \omega_e I_{sq} + \frac{1}{L_s}V_{sd} \\ \frac{dI_{sq}}{dt} = -\frac{R_s}{L_s}I_{sq} - \omega_e I_{sd} - \frac{1}{L_s}\omega_e\varphi + \frac{1}{L_s}V_{sd} \end{cases} \quad (5)$$

Where: the direct element of stator current is ( $I_{sd}$ ), the direct element of stator voltage is ( $V_{sd}$ ), the quadrature element of stator current is ( $I_{sq}$ ) and quadrature element of stator voltage ( $V_{sq}$ ); the stator resistance ( $R_s$ ), the stator inductance ( $L_s$ ), the flux linkage of the permanent magnet ( $\varphi$ ) and ( $\omega_e$ ) rotor speed of the PMSG. [19]

In other parts, using the two arc axes machine inductance  $L_{sd}$ ,  $L_{sq}$  and the number of pole pairs  $n_p$ , the electromagnetic torque equation can be expressed following the next equation:

$$T_e = \frac{3}{2}n_p I_{sq} [(L_{sd} - L_{sq})I_{sd} + \varphi] \quad (6)$$

If  $L_{sd} = L_{sq} = L_s$ , it means that is cited in surface of permanent magnet synchronous generator. So, the electromagnetic torque becomes:

$$T_e = \frac{3}{2}n_p\varphi I_{sq} \quad (7)$$

### 2.3 Battery modelling:

The battery modelling is enforced in [20, 21]. The proposed model of battery includes a voltage source noted ( $E_0$ ) connected in series with a resistor  $R_b$ . the battery output voltage ( $V_b$ ) can be expressed by: (8). [20]

$$V_b = E - R_b I_b \quad (8)$$

Where:

$E$ : the battery open circuit voltage.

$I_b$ : presents battery current.

Then, the open circuit voltage can be calculated using the next formula:

$$E = E_0 - K \frac{Q}{Q - \int I_b dt} + A \exp(-B \int I_b dt) \quad (9)$$

where:  $E_0$  is the constant battery voltage,  $K$ : is the battery polarization voltage,  $Q$ : is the capacity of the battery.  $\int I_b dt$ : is the real battery charge,  $A$ : is the exponential zone amplitude,  $B$ : is the exponential zone time constant inverse.

### 2.4 Super-capacitor modelling:

The SC is an innovative technic in storage field technics, which the energy storage process depends on the static charge, it's different to the battery storage method characterized by electro-chemical process [22]. The output SC voltage can be expressed using the next equation:

$$U_{SC} = N_{S-SC} (V_1 + R_1 \frac{I_{SC}}{N_{P-SC}}) \quad (10)$$

Where:  $U_{SC}$  and  $I_{SC}$  are respectively the SC voltage and current.  $V_1$ : the elementary SC voltage and lastly,  $N_{P-SC}$ : the number of parallel branches of the SC connections and  $N_{S-SC}$ : the number of series branches of the SC connections.

## 3. System control:

### 3.1 APO MPPT control techniques:

The Fig. 5 presents the adaptive perturb and observe control applied to the PV panels via the DC booster. The aim of the SMC is developing the PV voltage to track the  $V_{ref}$  given by APO method. This technique can extract and follow the maximum of produced power under varying meteorological conditions depending to the measurements of PV outputs current and voltage [26]. The algorithm flow chart showed in Fig. 5 discuss the principle of this method can be expressed by:

$$V(k) = V(k - 1) + k_{pV} [sign(\Delta P)] \quad (12)$$

And the  $\Delta P$  calculated using the difference between the actual and previous PV power:

$$\Delta P = P(k) - P(k - 1) \quad (13)$$

The  $k_{PV}$  presents the adaptive step gain, it can determine depending to the state of power variation, and  $V$  desire the output PV voltage.

In other parts, the construction of the control law requires a deep characterization of the system using the compoment of the PV boost converter, the next equation discuss the electric relation between the photovoltaic output and input of DC/DC boost (it is imposed  $R_s=0$  and  $R_{sh}=\infty$ ):

$$V = \frac{I_{PV}}{C_{PV}} - \frac{I_{dc}}{C_{PV}} \cdot u \tag{14}$$

Where:  $I_{pv}$ : output PV current and  $I_{dc}$ : boost current.

To build and design the SMC for the boost DC-DC converter. The next sliding surface as a linear mélange of variable states which can expressed using Eq. (15):

$$S = a_1x_1 + a_2x_2 + a_3x_3 \tag{15}$$

Where the SMC control parameters are  $a_1, a_2$  and  $a_3$  and they referred as sliding coefficients. The state feedback variables are  $x_1, x_2$  and  $x_3$ , and they defined following the next equations:

$$\begin{cases} x_1 = V_{PV-ref} - V_{PV} \\ x_2 = \frac{d(V_{PV-ref} - V_{PV})}{dt} \\ x_3 = \int (V_{PV-ref} - V_{PV}) dt \end{cases} \tag{16}$$

The  $u$  designs the SMC control law for the DC-DC boost converter, which:

$$u = \begin{cases} 1 & \text{if } S_{PV} > k \\ 0 & \text{if } S_{PV} < -k \end{cases} \tag{17}$$

Where, the constant  $k$  is an arbitrarily small value. The hysteresis band and the boundary conditions ( $S=k$  and  $S=-k$ ) can precise the form control of the switching frequency of the boost converter, thus solving the practical problem of a very high frequency switching operation. Furthermore, we choose in this article to work with SMC boost converter operations with constant frequency switching which it employs a PWM instead of hysteresis modulation.

### 3.2 PMSG generator control:

The Fig. 6 bellow details the structure of the PMSG control depending on the SMC controller. ( $I_{sq}$ ) reference is produced using the maximum

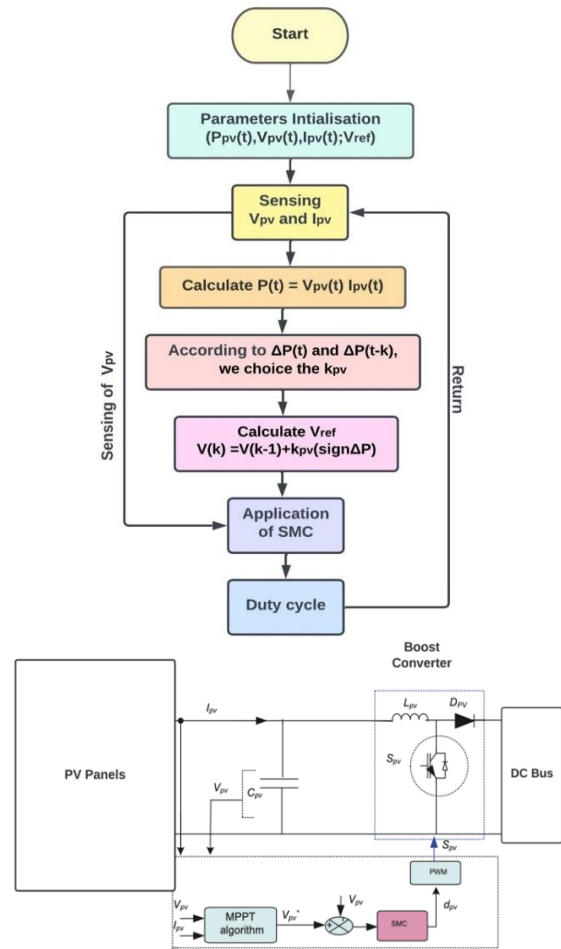


Figure. 5 APO flowchart and PV MPPT control

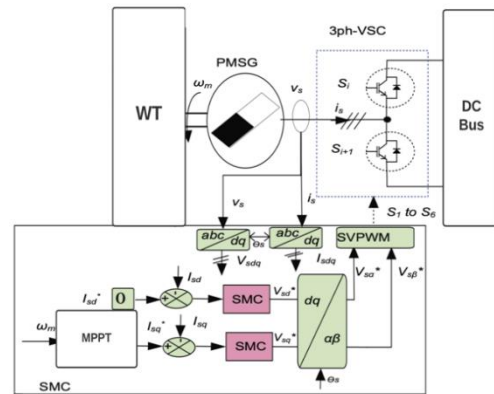


Figure. 6 Schematic of PMSG control

power point tracking given by Eq. (12); ( $I_{sd}$ ) reference is given 0 to verify the condition of power unity.

The error between ( $I_{sd}$  and  $I_{sd-ref}$ ;  $I_{sq}$  and  $I_{sq-ref}$ ) is measured and complete the reference elements for the SMC controller. The last one outputs was transformed from d-q to a-b frame, the obtained forms were transformed to 6 signals to command the VSC using the space vector modulation SVM [28]. The SMC inputs are expressed by:

$$\begin{cases} S_{s1} = I_{sd-ref} - I_{sd} \\ S_{s2} = I_{sq-ref} - I_{sq} \end{cases} \quad (18)$$

Where, the  $I_{sd-ref}$  and  $I_{sq-ref}$  represent the references values of variables  $I_{sd}$  and  $I_{sq}$ , respectively. It is necessary for control law that the sliding mode presence condition for the both surfaces is  $S_{si}S'_{si} < 0$ .

The structure of the control input can be calculated like:

$$\begin{cases} u_{s1} = u_{eqs1} + k_{s1}|S_{s1}|^a \text{sgn}(S_{s1}) \\ u_{s2} = u_{eqs2} + k_{s2}|S_{s2}|^a \text{sgn}(S_{s2}) \end{cases} \quad (19)$$

The positive parameters of (k and a) can help to enhance the switching speed at time of the system operate away from the sliding surface. However, the information control  $u_{eqsi}$  is calculated depending to the invariance condition using the accompanying condition, which  $S_{si}$  and  $S'_{si} = 0 \rightarrow u_{si} = u_{eqsi}$ . The final expression of the control form  $u_{eqsi}$  is presented by the next equation:

$$\begin{cases} u_{q1} = (R_s I_{sd} - w_e L_q I_{sq}) + L_d I'_{sd-ref} \\ u_{q1} = (R_s I_{sq} + w_e \frac{L_d}{L_q} I_{sd} + w_e \Psi) + I'_{sq-ref} \end{cases} \quad (20)$$

### 3.3 Battery control modelling:

The schematic in Fig. 7 investigates the details of converter control tied to the battery, it depends to the sliding mode control controller.

The current regulation of switches converter (Sb-1, Sb-2) needs firstly a definition of the sliding surface using the next equation [29]:

$$S_b = \delta_1 y_1 + \delta_2 y_2 + \delta_3 y_3 \quad (21)$$

Where:

( $\delta, \delta_2, \delta_3$ ) are the three principal parameters of the sliding mode control, they depend to sliding

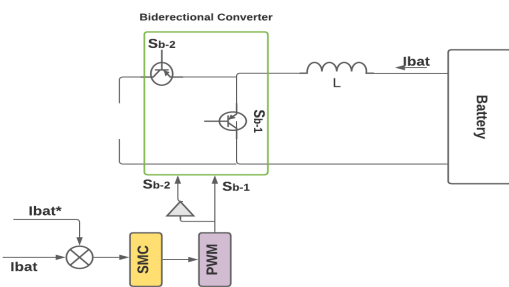


Figure. 7 The battery schematic control

coefficients which can precise the state feedback of  $y_1, y_2$  and  $y_3$  variables. Also, they present a positive value extracted from the solutions of differential equation depending to a location root.

The general expressions of these variables are:

- First variable  $y_1$ :

$$y_1 = I_{bat-ref} - I_{bat} \quad (22)$$

- Second variable  $y_2$ :

$$y_2 = \frac{d(I_{bat-ref} - I_{bat})}{dt} \quad (23)$$

- Third variable  $y_3$ :

$$y_3 = \int (I_{bat-ref} - I_{bat}) dt \quad (24)$$

Where: ( $I_{bat-ref}$  and  $I_{bat}$ ) express respectively the reference and measured battery current.

### 3.4 Super-capacitor control modelling:

The Fig. 8 details the SMC control of the converter coupled to the SC. Furthermore, the converter switches control depends to the input current regulation (Ssc-1, Ssc-2), needs a deep definition the sliding surface using Eq. (19) [30]:

$$S_{sc} = \theta_1 x_1 + \theta_2 x_2 + \theta_3 x_3 \quad (25)$$

Where: ( $\theta_1, \theta_2, \theta_3$ ) present the SMC control parameters, they utilized the sliding coefficients for specifying the state feedback of  $x_1, x_2$  and  $x_3$  variables. Also, these variables take a positive value obtained by solving a differential equation solution depending to the location root.

The general expressions of these variables are:

- First variable  $x_1$ :

$$x_1 = I_{sc-ref} - I_{sc} \quad (26)$$

- Second variable  $x_2$ :

$$x_2 = \frac{d(I_{sc-ref} - I_{sc})}{dt} \quad (27)$$

- Third variable  $x_3$ :

$$x_3 = \int (I_{sc-ref} - I_{sc}) dt \quad (28)$$

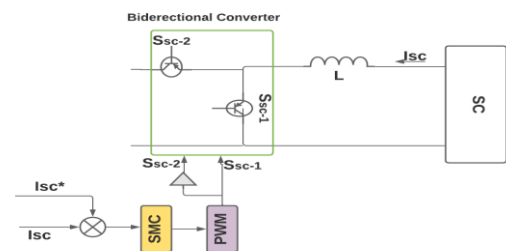


Figure. 8 Supercapacitor schematic control

Where: ( $I_{SC-ref}$  and  $I_{sc}$ ) present respectively the reference and output supercapacitor current.

### 3.5 The control of VSI:

The proposed VSI control based on the SMC illustrated in Fig. 9. The control depends to the PV output power, grid side current / voltage. The control operation starts with comparison between grid side current ( $I_g$ ) and reference current ( $I_{ref}$ ) as showed in Fig. 9. The obtained error can be corrected using two principal SMC controllers, and send two corrected signals of the voltage compositions to the SVPWM in the reference  $\alpha$ - $\beta$  depending to the reverse of Park transformation [30, 31].

The calculated direct reference current ( $I_{d-ref}$ ) depends to the active power injected into the grid ( $P_{i-ref}$ ):

$$I_{d-ref} = \frac{P_{i-ref}}{V_g} \quad (29)$$

Also, the reference current ( $I_{q-ref}$ ) can be calculated using the reactive power injected into the grid ( $Q_{i-ref}$ ):

$$I_{q-ref} = \frac{Q_{i-ref}}{V_g} \quad (30)$$

We convert the 3-phase grid current form to dq current form. Finally, the sliding surface expressed by:

$$\begin{cases} S_{id} = I_{d-ref} - I_{id} \\ S_{iq} = I_{q-ref} - I_{iq} \end{cases} \quad (31)$$

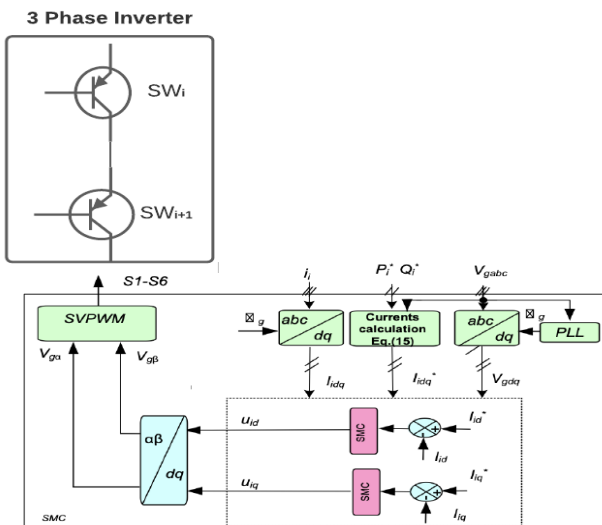


Figure. 9 VSI schematic control

The general structure of the input control is:

$$\begin{cases} U_{id} = U_{eq-g1} + K_{g1} |S_{id}|^\alpha \text{sgn}(S_{id}) \\ U_{iq} = U_{eq-g2} + K_{g2} |S_{iq}|^\alpha \text{sgn}(S_{iq}) \end{cases} \quad (26)$$

Which, the elementary control terms  $U_{eq-g1}$  and  $U_{eq-g2}$ , and the ranges of switching gain are:

$$U_{eq-g1} = R_1 I_{id} - L_1 \omega I_{iq} + V_{1d} \quad (32)$$

And

$$U_{eq-g2} = R_1 I_{iq} - L_1 \omega I_{id} + V_{1q} \quad (33)$$

And

$$K_{g1} > L_1 |\Delta f_{g1}| \quad (34)$$

And

$$K_{g2} > L_1 |\Delta f_{g2}| \quad (35)$$

The gain values have an important rule to specify the convergence of  $S_{si}$  to zero.

### 3.6 Power flow control:

The proposed algorithm of the power flow depends to different sources, storage components, load demand and climate conditions. The process starts by sensing the battery SOC, PV output power ( $P_{pv}$ ), wind power ( $P_w$ ) battery power ( $P_{bat}$ ), supercapacitor power ( $P_{sc}$ ), grid power ( $P_g$ ) and load power ( $PL$ ). The algorithm divided on two parts depending to the grid modes. The main roles of the proposed power flow management algorithm are reducing the grid dependence and maximizing the self-consumption which has an important effect like the low costs operating and low gazes' emissions. Besides that, it is necessary to remind that this algorithm is oriented to reduce the battery dynamic stress which can enhance their lifespan and reduce the degradation costs. However, this paper includes two grid configurations modes such as the isolated (stand-alone) mode and the grid-ON mode:

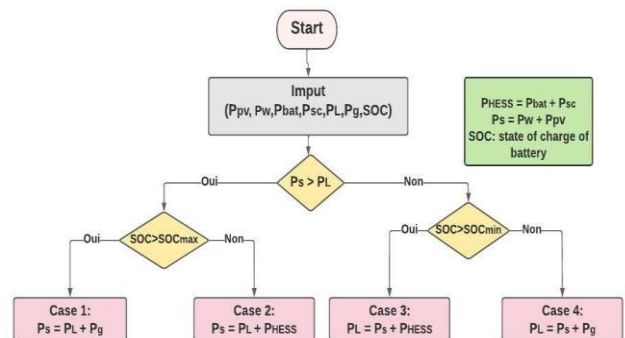


Figure. 10 Flowcharts of the power system

### 3.6.1. Case of isolated mode (grid-off):

The aim of this case is minimizing the dependence and consumption from the grid. Under a good climate conditions, the hybrid sources (photovoltaic - wind turbine) can produce an important energy able to feed sufficiently the load and deliver a part of energy to the storage bank ( $SOC < SOC_{max}$ ) (second scenario) in Fig. 11. At time of low PV and WT production, the storage system delivers the necessary power to the load (third scenario).

### 3.6.2. Case of HRES system tied to the grid:

In this case we work under good climate conditions, the sources produce the necessary power for the load and inject the other part of power into the grid, also the battery in this point achieved the maximum of SOC ( $SOC > SOC_{max}$ ) (first scenario) in Fig. 10. The last scenario imposes the dependence of grid utility because the PV and wind turbine sources and storage elements cannot deliver the necessary energy to the load (fourth scenario), that's involves the grid power sharing.

## 4. Simulation results and discussion:

To analyze the dynamic performance and effectiveness of the HRES, we propose a series of simulation experiences under different grid modes. The proposed HRES is composed, simulated and discussed using M. SIMULINK and SAM. The solar irradiance profile variate from (500 w/m<sup>2</sup> to 1000 w/m<sup>2</sup>), (1000 w/m<sup>2</sup> to 600 w/m<sup>2</sup>), the temperature is fixed at 25°C. In other part, the uncertainties are formalized in the proposed model because the SMC is necessary be robust against uncertain parameters. For the filter (LCL) components and the values of parametric variations ( $RI$ ,  $LI$ ) are specifying at 5% of its maximum value. Also, the convergence condition of SMC only calculates the range of coefficient  $k$ ; the values are adjusted by simulation considering uncertain parameters, the speed of response without significant overshoot, reduction of the amplitude of oscillations and static error.

### 4.1 First case: Isolated mode HRES with variable inputs and load demand:

The first simulation part is considered as stand-alone mode which includes two principals cited scenarios in Fig. 10. The Fig. 11 presents the solar irradiance profile applicated on the PV panels during simulation operating and the photovoltaic output current  $I_{pv}$ , voltage  $V_{pv}$  and power  $P_{pv}$

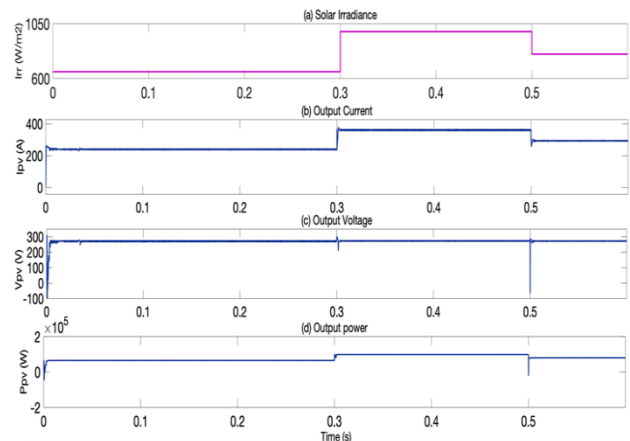


Figure. 11 Photovoltaic outputs

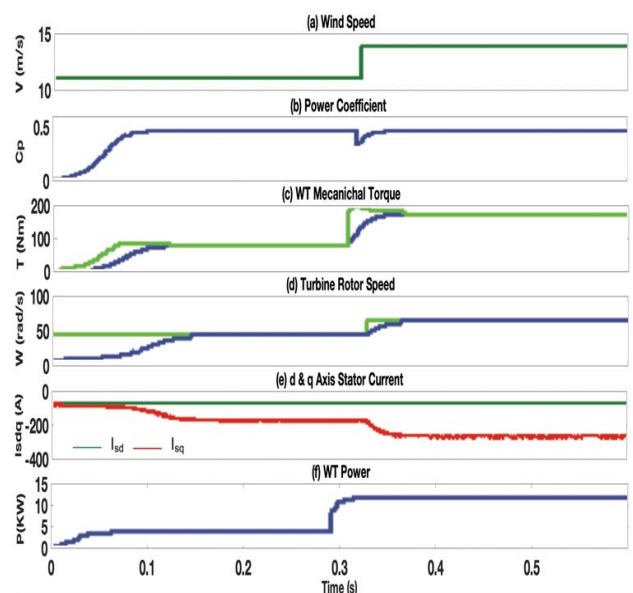


Figure. 12 Wind turbine outputs parameters

under the proposed conditions. In the other parts, during the quick solar irradiance changing, it is remarked, the PV system is able to deliver the max of power and present a high performance which show the effectiveness and capability of the APO as a MPPT. Besides that, the APO can follow the MPP with high precision under varying meteorological conditions.

For the second source, the Fig. 12 analyze the performance of the wind turbine system which includes the wind speed profile applicated of the turbine (a), the coefficient of power (b), (c) presents respectively the measured rotor speed and reference rotor speed of the PMSG, (d) illustrates a comparison between the reference and output torque of the WT and (e) shows the output power of the WT. The obtained graphs in the Fig. 12 confirm that the proposed PMSG controller operates in the MPP regardless to the variable wind speed, system oscillations and load demand.

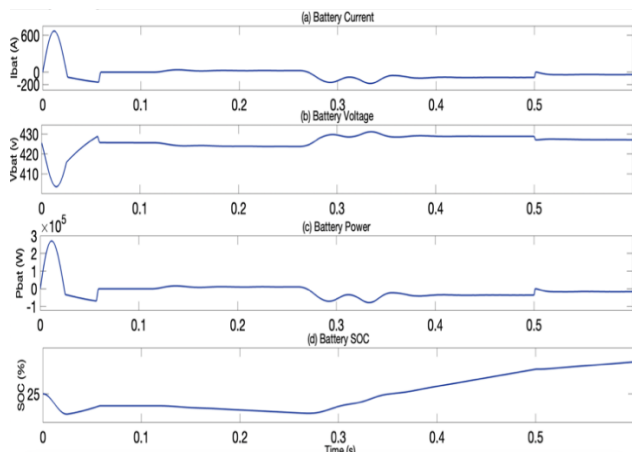


Figure. 13 Battery outputs

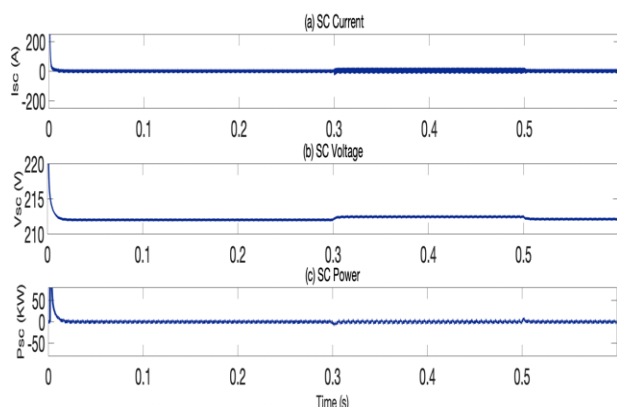


Figure. 14 Supercapacitor outputs

The Fig. 13 shows the battery response during the simulation operating, which contains the principal battery parameters such as the voltage (a), current (b), power (c) and state of charge (SOC%) (d). In the period [0; 0.3] s, the battery remarks a negative power that is explained by the high-power generation by the PV system and wind turbine. So, in this period the hybrid sources are able the feed sufficiently the load and deliver energy to the storage banks. In the next period of simulation, the battery remarks positive power which it is explained by the low production of the sources or one of them. The obtained results confirm two important ideas proposed in flowchart Fig. 10. Besides that, the battery presents a fable oscillation under varying system conditions which show the effectiveness and capability of the SMC controller of the bidirectional converter.

The Fig. 14 presents the SC output current, voltage and power, it demonstrates the principal role of using supercapacitor, it can absorb the system fluctuations delivered by different power system issues which it is clearly showed in graphs (a) and (b) during 0.3s and 0.5s. The SC has a positive impact on the battery, it can reduce the battery stress, minimize the battery degradation.

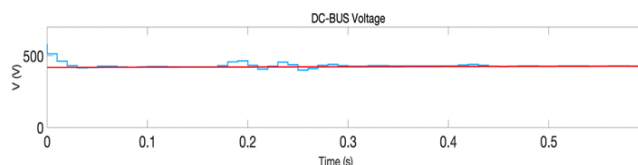


Figure. 15 DC-link bus voltage

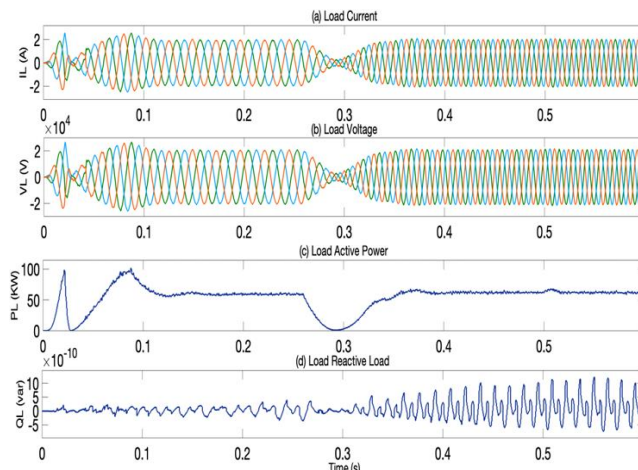


Figure. 16 Load performance

The Fig. 15 investigate a comparison between the measured capacitor link voltage and the proposed reference DC capacitor bus voltage, they present a high similarity of the both voltage values during the simulation period which explain the capability of the proposed HERS control. The Fig. 16 shows the load 3-phase current, 3-phase voltage, active power and reactive power. It is remarked that the current and voltage are in phase under varying conditions, also the load current and voltage presents a low harmonics distortion, the injected load reactive power is very fable ( $\sim 0$  Var) during system operating which confirm the great performance of the proposed SMC controller of VSC.

To confirm the obtained results in this case and appreciate the proposed control, we applicate a different comparatives tests between the PI, SMC and Hysteresis Current controllers, using SAM program. The comparison process based on produced harmonic distortion rate (THD) of the load voltage. Furthermore, the obtained values in Table 3 demonstrates the effectiveness and capability of the SMC controller face the both other controllers which presents more advantages like the low THD, fast steady-state error and voltage/current regulation.

Table 3. the THD values of PI and SMC and hysteresis current controller

Test	Parameters	Hysteresis	PI	SMC
1	THD (0;0.3) s	3.72 %	3,85 %	0,13 %
2	THD (0.3;0.5) s	4.63 %	4.92 %	1,88 %
3	THD (0.5;0.6) s	3.98%	4.05 %	3.43 %

### 4.2 Second case: HERS tied to the grid utility:

In this part, we execute the proposed HRES controller under varying meteorological conditions as the solar irradiation and wind speed featuring mode grid on. The Fig. 17 illustrates the APO and SMC controller performance of the photovoltaic system under variable solar data. It is remarked that the photovoltaic controller produces the maximum of generated power under quick variation of meteorological conditions, which show the effectiveness and capability of the considered APO algorithm as MPPT.

The Fig. 18 presents the response of the second source of the proposed HRES correspond to the WT, it's showing the wind speed profile applied on the turbine (a), the coefficient of power (b), (c) presents respectively the measured rotor speed and reference rotor speed of the PSMG, (d) illustrates a comparison between the reference and output torque

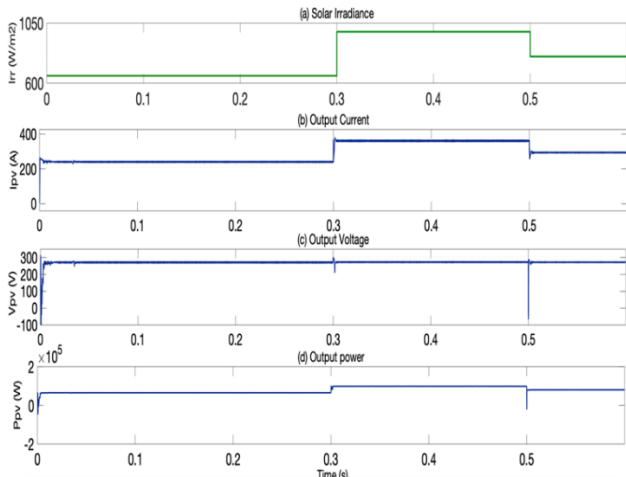


Figure. 17 PV outputs

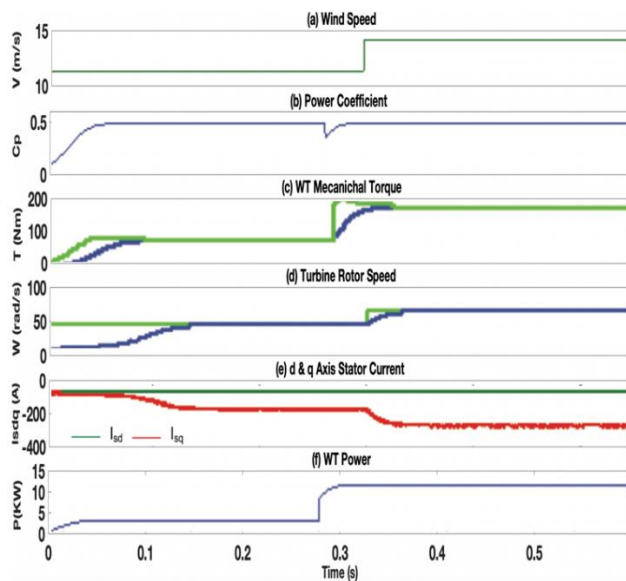


Figure. 18 Wind turbine outputs

of the WT and (e) shows the output power of the WT. It is observed that the designed control of this source presents an important result which make the WT presents a high performance and generate the optimal power during the quick changing of the environmental conditions and grid faults.

The Fig. 19 illustrates the battery storage response, it's contains the battery current (a), voltage (b), power (c) and SOC (d). during the period [0;0.3] s, the battery still out of operating due to low SOC < SOC<sub>min</sub> and the sources produce insufficient power, according to this problem the grid shares the needed power for the load (scenario 4). Then, the time period between (0.3s and 0.5s), the sources create a sufficient power which can feed the load (scenario2), it's showed in Fig. 19, the battery current curve take a negatives values which design the charging operation.

The Fig. 20 illustrates the SC current, voltage and power variations curves, which the SC current curve investigates the main rule of SC absorb the high system fluctuation caused by irradiance variations and load and grid demand which can protect the battery and them enhance lifespan.

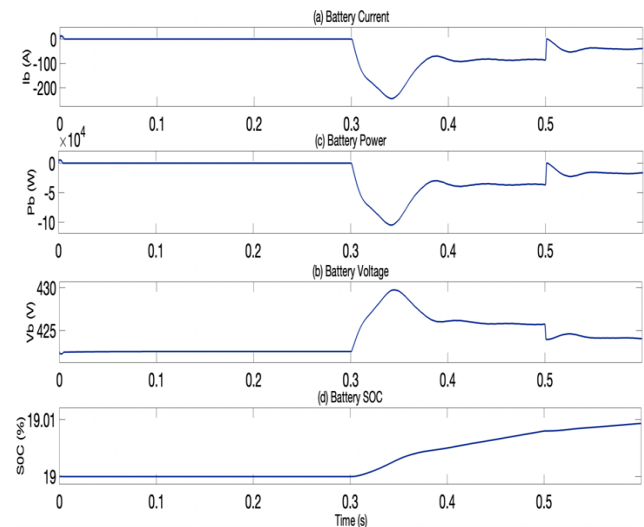


Figure. 19 Battery outputs

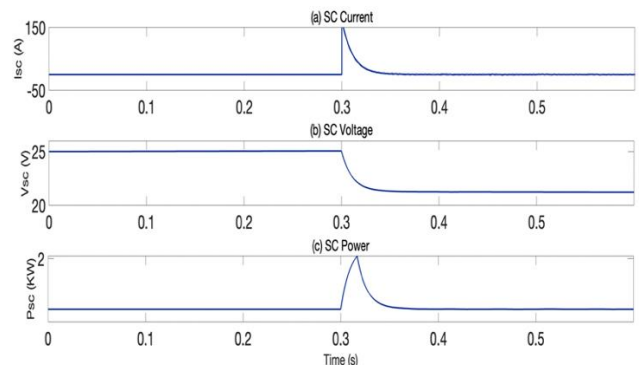


Figure. 20 SC outputs

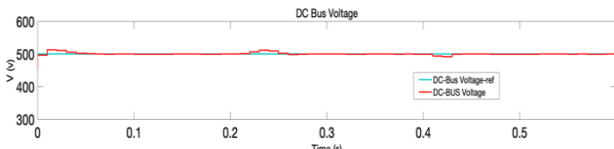


Figure. 21 DC-BUS link voltage

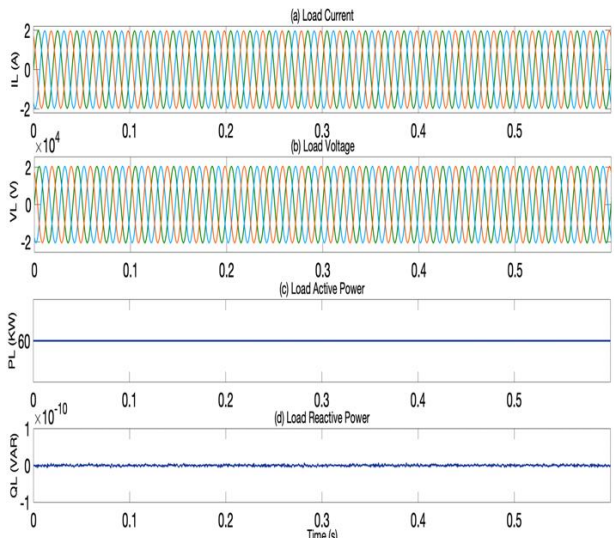


Figure. 22 Load performance

Table 4. The THD values of PI and SMC and hysteresis current controller

Test	Parameters	Hysteresis	PI	SMC
1	THD (0;0.3) s	10.98 %	11.75%	3.97 %
2	THD (0.3;0.5) s	9.46 %	9.89 %	2.02 %
3	THD (0.5;0.6) s	10.98 %	12.86%	4.88 %

The Fig. 21 compares between the measured DC capacitor bus voltage and the reference DC capacitor voltage, it is remarked a high similarity of the both voltage values during the simulation periods which explain the capability and effectiveness of the proposed HERS control.

In this part of simulation, it is fixed the load power demand at 60 KW, the Fig. 22 presents the measured electrical parameters, we observe that the 3-phases of current and voltage were respectively in phase, also, the delivered reactive power is very fable. Therefore, the obtained results in this figure demonstrate the feasibility and capability of the used control

The Fig. 23 shows respectively current, voltage, grid active and reactive power. The grid shares the necessary power to the system when the principal's sources are incapable to feed the load. The grid active power curve presents a negatives values, it confirms that the grid utility deliver power to the system. Besides that, the 3-phases form of grid current and voltage are in phase accompanied with low harmonic distortion (THD). Finally, the obtained results concerning second case of

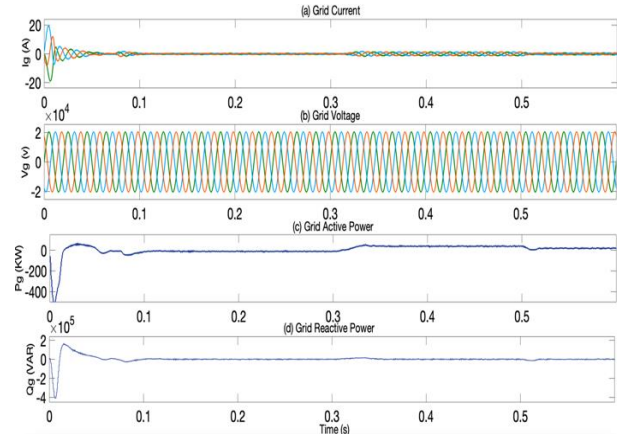


Figure. 23 Grid utility performance

simulation validate the performance and effectiveness of the proposed the HRES control.

In other part, to complete and validate the performance of the proposed HERS system control, it is realized a series of comparatives tests using SAM program contain: the proposed SMC, PI and hysteresis current controllers. The next table 4 includes the obtained comparison results in SAM program. we observe that the THD output values measured of the inverter voltage based on the SMC technic are lower than 5% compared to the other controller. Finally, the proposed sliding mode control of this paper presents a perfect effect on the power quality of the proposed hybrid renewable energy system compared to the others controllers.

### 5. Conclusion:

This paper tries to study and validate the proposed contribution of the SMC control applied on hybrid renewable energy system composed by PV generators, wind turbine, battery and super-capacitor featuring isolated mode and grid-ON mode depending to the SMC as the manager of the power into the system. The obtained results in the both cases confirm and validate the adequacy and effectiveness of the proposed SMC control applied on the power converters under varying solar irradiance, grid and load problems. Also, it is capable to manage the system power resources with high performance, the APO control able to extract the MPP under varying meteoritical conditions, the PMSG control extract the max of power and the VSC & bidirectional converters are adapted and controlled with high effectiveness. Besides that, this work shows the important rule of the SC to reduce the battery stress and enhance their lifespan by absorbing the system fluctuations. Finally, these rated results of simulations using the proposed SMC control applied on the HRES provide many

advantages such as fast-steady state, low THD and robustness.

### Conflicts of Interest

The authors declare no conflict of interest.

### Author Contributions

Z. Abousserhane, as the corresponding author, has designed the proposed HRES control. Also, he has modelled and implemented the proposed system using MATLAB/Simulink. A. Abbou has supervised the written paper and providing the necessary advices. H. Bouzakri has contributed to the writing and the paper organization. All authors approved the final version.

### References

- [1] S. Rajamand, M. S. Khah, and J. Catalao, "Energy storage systems implementation and photoVoltaic output prediction for cost minimization of a Microgrid", *Electric Power System Research* 2022, 107596, 2022.
- [2] M. Akil, E. Dokur, and R. Bayindir, "Energy Management for EV Charging Based on Solar Energy in an Industrial Microgrid", In: *Proc. of 2020 9th International Conference on Renewable Energy Research and Application*, pp. 489-493, 2020.
- [3] M. Hemmati, M. A. Mirzaei, M. Abapour, B. Ivatloo, H. Mehrjerdi, and M. Marzband, "Economic-environmental analysis of combined heat and power-based reconfigurable microgrid integrated with multiple energy storage and demand response program", *Sustain. Cities Soc.* 69. SP., 102790, 2021.
- [4] H. Queiroz, R. A. Lopesn, and J. Martins, "Automated energy storage and curtailment system to mitigate distribution transformer aging due to high renewable energy penetration", *Electric Power System Res.*, 182, 106199, 2020.
- [5] H. Bouzakri, A. Abbou, K. Tijani, and Z. Abousserhane, "Biaxial Equatorial Solar Tracker with High Precision and Low Consumption: Modelling and Realization", *International Journal of Photoenergy*, Vol. 2021.
- [6] S. Álvarez and J. Espinosa, "Multi-Objective Optimal Sizing Design of a Diesel–PV–Wind–Battery Hybrid Power System in Colombia", *International Journal of Smart Grid*, Vol. 2, No. 1, 2018.
- [7] H. Shahinzadeh, M. Moazzami, S. Fathi, and G. B. Gharehpetian, "Optimal sizing and energy management of a grid-connected microgrid using HOMER software", *Smart Grids Conference, IEEE*, pp. 1-6, 2016.
- [8] M. A. Elgendy, B. Zahawi, and D. J. Atkinson, "Assessment of perturb and observe MPPT algorithm implementation techniques for PV pumping applications", *IEEE Transactions on Sustainable Energy*, 3(1), 21-33, 2012.
- [9] S. G. Malla and N. Bhende, "Voltage control of stand-alone wind and solar energy system", *International Journal of Electrical Power and Energy Systems*, 56, pp. 361-373, 2014.
- [10] A. Rezvani, A. Khalili, A. Mazareie, and M. Gondomar, "Modeling, control, and simulation of grid connected intelligent hybrid battery/photoVoltaic system using new hybrid fuzzy-neural method", *ISA Transactions*, 63, pp. 448-460, 2016.
- [11] A. F. Nematollahi, H. Shahinzadeh, H. Vahidi, B. Amirat, and Y. M. Benbouzid, "Sizing and Sitting of DERs in Active Distribution Networks Incorporating Load Prevailing Uncertainties Using Probabilistic Approaches", *Applied Sciences*, Vol. 11, No. 9, 4156, 2021.
- [12] A. Dendouga, "Conventional and Second Order Sliding Mode Control of Permanent Magnet Synchronous Motor Fed by Direct Matrix Converter: Comparative Study", *Energies*, Vol. 13, No. 19, p. 5093, 2020.
- [13] S. S. Ullah, Z. Ali, and J. S. Ro, "A Super Twisting Fractional Order Terminal Sliding Mode Control for DFIG-Based Wind Energy Conversion", *System, Energies*, Vol. 13, No. 9, 2020.
- [14] C. J. Q. Teh, M. Drieberg, S. Soeung, and R. Ahmad, "Simple PV Modeling Under Variable Operating Conditions", *IEEE Access*, Vol. 9, pp. 96546-96558, 2021.
- [15] I. Grgić, M. Bašić, D. Vukadinović, and M. Bubalo, "Optimal Control of a Standalone Wind-Solar-Battery Power System with a Quasi-Z-Source Inverter", In: *Proc. of 9th International Conference on Renewable Energy Research and Application*, pp. 61-66, 2020.
- [16] Z. Liang, A. Q. Huang, and R. Guo, "High efficiency switched capacitor buck-boost converter for PV application", In: *Proc. of Annual IEEE Applied Power Electronics Conference and Exposition*, pp. 1951-1958, 2012.
- [17] Z. Kan, Z. Li, and M. Yi, "Research on Grid-Connected/Islanded Control Strategy of PV and Battery Storage Systems as Emergency Power

- Supply of Pumping Storage Power Station”, In: *Proc. of 3rd International Conference on Electronics Technology*, pp. 457-462, 2020.
- [18] H. Bouzakri, A. Abbou, and K. Chennoufi, “Efficiency Enhancement of a Fixed PhotoVoltaic Panel Using Simple Motorized Reflection Model”, *International Journal of Intelligent Engineering and Systems*, Vol. 14, No. 4, pp. 77-90, 2021, doi: 10.22266/ijies2021.0831.08.
- [19] Z. Abousserhane, A. Abbou, and H. Bouzakri, “Developed Power Flow Control of PV/Battery/SC Hybrid Storage System Featuring Two Grid Modes”, *Inter. Journal of Renewable Energy Research*, Vol. 12, No. 1, 190-199, 2022
- [20] G. A. Raiker, U. Loganathan, and S. Reddy, “Current Control of Boost Converter for PV Interface With Momentum-Based Perturb and Observe MPPT”, *IEEE Transactions on Industry Applications*, Vol. 57, No. 4, pp. 4071-4079, 2021.
- [21] D. Aranzazu and M. Jesus, “Backstopping Controller Design to Track Maximum Power in PhotoVoltaic Systems”, *Automatika Journal*, Vol. 55, No. 1, 22-3, 2014.
- [22] Y. Sun, Z. Zhao, M. Yang, D. Jia, W. Pei, and B. Xu, “Overview of energy storage in renewable energy power fluctuation mitigation”, *CSEE Journal of Power and Energy Systems*, Vol. 6, No. 1, pp. 160-173, 2020.
- [23] M. Brenna, M. Longo, W. Yaici, and D. Abegaz, “Simulation and optimization of integration of hybrid renewable energy sources and storages for remote community’s electrification”, *IEEE PES Innovative Smart Grid Technologies Conference Europe*, pp. 1-6, 2017.
- [24] Z. Abousserhane, A. Abbou, and H. Bouzakri, “Effective Power Management of PV/Battery Hybrid System Under Varying Frequency Modes”, In: *Proc. of 2nd International Conference on Innovative Research in Applied Science, Engineering and Technology*, pp. 1-8, 2022.
- [25] T. Abderrahim and B. Said, “Control and management of grid connected PV-Battery hybrid system based on three-level DCI”, In: *Proc. of 6th International Conference on Systems and Control*, pp. 439-444, 2017.
- [26] S. Marhraoui, A. Abbou, Z. Cabrane, S. Rhaili, and N. E. Hichami, “Fuzzy Logic-Integral Backstepping Control for PV Grid-Connected System with Energy Storage Management”, *International Journal of Intelligent Engineering and Systems*, Vol. 3, 359-372, 2020, doi: 10.22266/ijies2020.0630.33.
- [27] A. F. Shahinzadeh, H. Nafisi, H. Vahidi, B. Amirat, and M. Benbouzid, “Sizing and Sitting of DERs in Active Distribution Networks Incorporating Load Prevailing Uncertainties Using Probabilistic Approaches”, *Applied Sciences*, Vol. 11, No. 9, 4156, 2021.
- [28] N. K. S. Naidu and B. Singh, “Grid-Interfaced DFIG-Based Variable Speed Wind Energy Conversion System with Power Smoothing”, *IEEE Trans. Sustain. Energy*, 8, 51-58, 2017.
- [29] Z. Abousserhane, A. Abbou, L. I. Khajine, and N. E. Zakzouk, “Power Flow Control of PV System Featuring On- Grid and Off-Grid Modes”, In: *Proc. of 7th Inter. Renewable and Sustainable Energy Conference*, pp. 1-7, 2019.
- [30] S. G. Malla and C. N. Bhende, “Voltage control of stand-alone wind and solar energy system”, *International Journal of Electrical Power & Energy Systems*, 56, pp. 361-373, 2014.
- [31] C. Ammari, D. Belatrache, B. Touhami, and S. Makhoulfi, “Sizing, optimization, control and energy management of hybrid renewable energy system- a review”, *Energy Built Environ*, S2666-1233(21)00030-1, 2021.
- [32] L. W. Chong, W. Wong, K. Rajkumar, and D. Isa, “An Optimal Control Strategy for Standalone PV System with Battery-Supercapacitor Hybrid Energy Storage System”, *Journal of Power Sources*, Vol. 331, pp. 553-565, 2016.